Biosci. Rep. (2013) / **33** / art:e00002 / doi 10.1042/BSR20120086

OPEN ACCESS

Original Paper

Role of Met^{58} in the regulation of electron/proton transfer in trihaem cytochrome PpcA from *Geobacter sulfurreducens*

Leonor MORGADO*, Joana M. DANTAS*, Telma SIMÕES*, Yuri Y. LONDER†[1], P. Raj POKKULURI† and Carlos A. SALGUEIRO*[2]

*Requimte-CQFB, Departamento de Química, Faculdade de Ciências e Tecnologia, Universidade Nova de Lisboa, Campus Caparica, 2829–516 Caparica, Portugal, and †Biosciences Division, Argonne National Laboratory, Argonne, IL 60439, U.S.A.

Synopsis

The bacterium Gs (*Geobacter sulfurreducens*) is capable of oxidizing a large variety of compounds relaying electrons out of the cytoplasm and across the membranes in a process designated as extracellular electron transfer. The trihaem cytochrome PpcA is highly abundant in Gs and is most probably the reservoir of electrons destined for the outer surface. In addition to its role in electron transfer pathways, we have previously shown that this protein could perform e^-/H^+ energy transduction. This mechanism is achieved by selecting the specific redox states that the protein can access during the redox cycle and might be related to the formation of proton electrochemical potential gradient across the periplasmic membrane. The regulatory role of haem III in the functional mechanism of PpcA was probed by replacing Met^{58}, a residue that controls the solvent accessibility of haem III, with serine, aspartic acid, asparagine or lysine. The data obtained from the mutants showed that the preferred e^-/H^+ transfer pathway observed for PpcA is strongly dependent on the reduction potential of haem III. It is striking to note that one residue can fine tune the redox states that can be accessed by the trihaem cytochrome enough to alter the functional pathways.

Key words: electron transfer, *Geobacter*, multihaem cytochrome, NMR site-directed mutagenesis

Cite this article as: Morgado, L., Dantas, J.M., Simões, T., Londer, Y.Y., Pokkuluri, P.R. and Salgueiro, C.A. (2013) Role of Met^{58} in the regulation of electron/proton transfer in trihaem cytochrome PpcA from *Geobacter sulfurreducens*. Biosci. Rep. **33**(1), art:e00002.doi:10.1042/BSR20120086

INTRODUCTION

Extracellular electron transfer is one the most remarkable features of the *Geobacter* species, by which they can reduce toxic or radioactive metals and convert renewable biomass into electricity [1]. These properties could conceivably be explored for practical applications by genetically engineering strains or by the functional optimization of key respiratory electron transfer chain components. Metal oxides such as those of Fe(III) and Mn(IV) are examples of extracellular electron acceptors whose reduction has an important role in the geochemistry of water-saturated soils and aquatic sediments through the release of dissolved Fe(II) and Mn(II) [2,3]. In addition, the ability of *Geobacter* to reduce U(VI) and other radionuclides can also have an important impact on the dissemination of these compounds in the environments [4–6].

The most emergent feature from the analysis of the six genomes of *Geobacter* species already sequenced is indubitably the large diversity of *c*-type cytochromes [7–10]. In fact, with the exception of *G. lovleyi*, other *Geobacter* species sequenced have approximately 100 *c*-type cytochrome genes per genome [7]. Despite this, the number of well-conserved *c*-type cytochrome families is small among the *Geobacter* species [7]. One of these well-conserved families is the PpcA family of trihaem periplasmic cytochromes. The *Gs* (*Geobacter sulfurreducens*) PpcA family is presently the only one studied in detail by genetic, functional and structural methods [11–21]. This family is composed by five 10-kDa cytochromes, designated PpcA–PpcE, that have a

Abbreviations used: EXSY, exchange spectroscopy; Gs, *Geobacter sulfurreducens*; HSQC, heteronuclear single-quantum coherence; NOESY, nuclear Overhauser enhancement spectroscopy; rmsd, root mean square deviation; 2D, two-dimensional.

[1] Present address: New England Biolabs, 240 County Road, Ipswich, MA 01938, U.S.A.

[2] To whom correspondence should be addressed (email csalgueiro@fct.unl.pt).

conserved overall fold and haem core [14,21]. With the exception of PpcC, the functional electron transfer mechanisms of these proteins have been characterized [20,22]. The results obtained suggested that PpcA and PpcD can couple e^-/H^+ transfer and may be involved in the generation of a proton electrochemical potential gradient across the periplasmic membrane [20]. Studies carried out on *Gs* with knock-out mutations of the genes encoding the PpcA family cytochromes showed that cellular U(VI) and Fe(III) reduction activities are affected [19]. Interestingly, PpcA and PpcD are the only members of this family that, when deleted, showed marked alterations in *Gs* phenotypic characteristics in presence of iron oxides [18,19]. The solution structure of PpcA was recently determined [14] and can be used for rational design of PpcA mutants, an essential step towards engineering variants of *Gs* with increased respiratory rates and the concomitant improvement in the biotechnological applications.

In the present work, we aimed to probe the putative regulatory role of haem III in the functional mechanism of PpcA as a natural follow-up of the observations obtained from the functional characterization of *Gs* PpcA family [20]. In that work, it was proposed that the relative high reduction potential value of haem III was crucial in selecting the microscopic redox states that the protein can access during its redox cycle and, thus, in establishing the preferential pathways for electron transfer. In PpcA, haem III is located between the other two haem groups at the bottom of a cleft sandwiched by two α-helices formed by residues Ala^{19}–Lys^{22} and Lys^{52}–Met^{58} (Figure 1). Given the location of residue Met^{58} at the end of the latter α-helix, pointing its side chain towards the interior of the cleft, it is conceivable that it might control the solvent accessibility of haem III and, concomitantly, regulate its reduction potential value. In the present study, this residue was replaced by serine (PpcAM58S), asparagine (PpcAM58N), aspartic acid (PpcAM58D) and lysine (PpcAM58K) to evaluate the effects of polarity and charge at this position. Each mutant was ^{15}N-labelled and its redox properties were determined using visible and NMR techniques. The comparison of the redox properties with those obtained for the wild-type cytochrome revealed the crucial role of residue Met^{58} in the functional mechanism of PpcA.

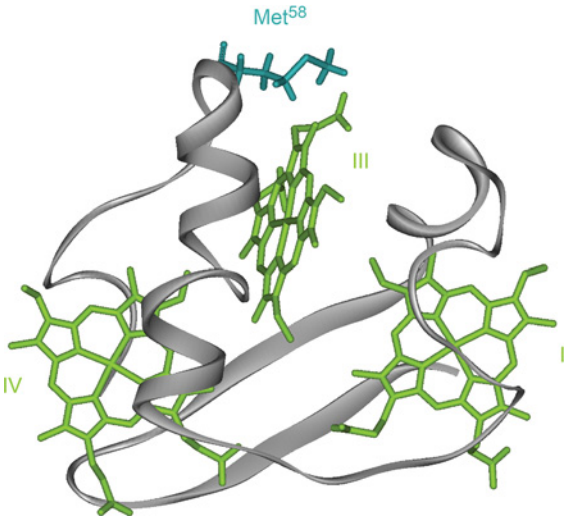

Figure 1 Location of residue Met^{58} in PpcA solution structure (PDB code 2LDO) [14]

The PpcA polypeptide chain (grey), haem groups (green) and the side chain of the methionine (blue) are represented. The haems are numbered I, III and IV, a designation that derives from the superimposition of the haems in cytochromes c_7 with those of the structurally homologous tetrahaem cytochromes c_3.

EXPERIMENTAL

Site-directed mutagenesis

For mutagenesis, the QuikChange Site-Directed Mutagenesis Kit (Stratagene) was used in accordance with the manufacturer's instructions. Oligonucleotides were synthesized by MWG Biotech. PpcA expression vector pCK32 [23] was used as a template. The presence of desired mutations was confirmed by DNA sequencing performed by MWG Biotech.

Bacterial growth and purification of PpcA mutants

Escherichia coli strain BL21(DE3) containing the plasmid pEC86 [24] was co-transformed with the expression vector containing the PpcA mutants (PpcAM58S, PpcAM58N, PpcAM58D or PpcAM58K). Transformed *E. coli* cells were grown in the 2×YT medium containing 34 μg/ml chloramphenicol and 100 μg/ml ampicillin. Protein expression was induced by adding IPTG (isopropyl β-D-thiogalactoside) to a final concentration of 10 μM. PpcA mutants were purified by cation exchange and gel filtration, as described for the wild-type cytochrome [17]. The purity of the proteins was evaluated by SDS/PAGE (15% gel), stained with Coomassie Brilliant Blue. To confirm the correct haem incorporation ESI–MS (electrospray ionization MS) was performed in the HHMI Biopolymer Laboratory and W.M. Keck Foundation Biotechnology Resource Laboratory at Yale University. Uniformly ^{15}N-labelled PpcA mutants were also expressed in *E. coli* as previously described [25]. Purification of labelled proteins was carried out as described above for unlabelled proteins.

NMR studies

Preparation of NMR samples

NMR samples and experimental conditions matched exactly those used in the characterization of the wild-type protein in the reduced and intermediate stages [20] and are summarized below. PpcAM58 mutant samples of about 140 μM for fully-reduced studies and 70 μM for redox titrations were prepared in 80 mM phosphate buffer with NaCl (250 mM final ionic strength) in ^2H_2O. Full reduction of the samples was achieved by the reaction with gaseous hydrogen in the presence of catalytic amounts of the enzyme Fe-hydrogenase, isolated from *Desulfovibrio vulgaris* (Hildenborough). Partially oxidized samples were obtained by first removing the hydrogen from the reduced sample with argon followed by the addition of controlled amounts of air into

the NMR tube. In the reduced and intermediate stages of oxidation, the pH was adjusted inside an anaerobic glove chamber with argon circulation to avoid sample reoxidation.

^{15}N-PpcAM58 mutant samples were prepared in 45 mM phosphate buffer (100 mM final ionic strength) in 92 % ^1H_2O/8 % ^2H_2O in the reduced state. Unlabelled samples were prepared under the same conditions.

NMR experiments and assignment

All the NMR experiments were performed on a Bruker Avance 600 spectrometer equipped with a TCI (triple-resonance cryoprobe). ^{1}H chemical shifts were calibrated using the water signal as internal reference and the ^{15}N chemical shifts calibrated through indirect referencing [26]. Spectra were processed using TOPSPIN (BrukerBiospin).

All the NMR experiments for the fully reduced samples were acquired under the same experimental conditions of wild-type [13,27]. The following set of experiments was acquired: ^{15}N-labelled samples in 92 % ^1H_2O/8 % ^2H_2O (298 K): 2D (two-dimensional)-^{1}H-^{15}N-HSQC (heteronuclear single-quantum coherence); unlabelled samples in 92 % ^1H_2O/8 % ^2H_2O : 2D-^{1}H-COSY, 2D-^{1}H-TOCSY (60 ms mixing-time) and 2D-^{1}H-NOESY (nuclear Overhauser enhancement spectroscopy; 50 ms); unlabelled samples prepared in ^2H_2O (288 K): 2D-^{1}H-TOCSY (45 ms) and 2D-^{1}H-NOESY (100 ms).

To monitor the stepwise oxidation of the individual haems in PpcAM58 mutants, 2D-^{1}H-EXSY (exchange spectroscopy) spectra in the pH range 6–9 were acquired in partially oxidized samples, as reported previously for the wild-type protein [20]. The program Sparky – NMR Assignment and Integration Software [28] – was used for inspection and for assignment of the signals in the NMR spectra. The specific assignment of haem signals to the respective haems in the reduced state in PpcAM58 mutants was performed using the methodology previously described for the wild-type protein [13,20]. The specific assignment of the backbone amide signals in PpcAM58 mutants was achieved using the assigned signals in the wild-type protein [27] as a guide.

Redox titrations followed by visible spectroscopy

Due to the negative reduction potentials of the haem groups, the redox titrations followed by visible spectroscopy of each PpcAM58 mutant were carried out inside an anaerobic chamber (MBraun) as described previously [13]. Samples with 18 μM protein concentration were prepared at pH 7 and 8 in NaCl/phosphate buffer solution with a final ionic strength of 250 mM. Both redox titrations were carried out at 288 K. The reduced fraction of the proteins was determined by integrating the area of the α-peak (551 nm) above the line connecting the flanking isosbestic points (543 and 559 nm) to subtract the optical contribution of the redox mediators, as described for the wild-type protein [13]. To check for hysteresis, each redox titration was performed in both oxidative and reductive directions. The experiments were performed at least twice, and the reduction potentials [relative to SHE (standard hydrogen electrode)] were found to be reproducible within $\pm$5 mV.

Thermodynamic model

In case of a trihaem cytochrome, three consecutive reversible steps of one-electron transfer convert the fully reduced state (stage 0, S_0) into the fully oxidized state (stage 3, S_3), and therefore four different redox stages can be defined, each group consisting of microstates with the same number of oxidized haems (see Supplementary Figure S1 at http://www.bioscirep.org/bsr/033/bsr033e002add.htm), as previously described [20]. The general theoretical framework that allows the detailed study of the redox centre thermodynamic properties in multihaem proteins was previously described [29] and was used to determine the thermodynamic parameters of the redox centres for the wild-type protein [20]. In summary, taking as reference the fully reduced and protonated protein, the energy of the microstates can be described over the full range of pH and solution potential as sums of ten parameters: the three energies of oxidation of the haems (reduction potentials), the pK_a of the redox–Bohr centre plus six two-centre interactions energies (three haem–haem and three redox–Bohr). In order to obtain such information it is necessary to monitor the stepwise oxidation of each haem using 2D-EXSY NMR experiments, which allow discriminating the individual haem signals in different oxidation stages [30,31]. The information obtained from the NMR data allows the determination of the thermodynamic parameters relative to the reference state (for a review see [29]).

In the characterization of the wild-type protein, the chemical shifts obtained for the haem methyls 12$^1CH_3^I$, 7$^1CH_3^{III}$ and 12$^1CH_3^{IV}$ (labelled according to the IUPAC nomenclature; see Supplementary Figure S2 at http://www.bioscirep.org/bsr/033/bsr033e002add.htm) in each oxidation stage in the pH range 6–9 were fitted simultaneously with visible redox titrations data obtained at pH 7 and 8.

In order to obtain thermodynamic parameters of the four PpcAM58 mutants the same set of haem methyls were used and visible redox titrations were performed under identical experimental conditions. The experimental uncertainty of the NMR data was evaluated from the linewidth of each NMR signal at half height; the visible data points were given an uncertainty of 3 % of the total optical signal.

RESULTS AND DISCUSSION

Impact of the mutations on the global fold and haem core

The yields of the four PpcAM58 mutants were similar to that obtained for the wild-type protein (approximately 3 mg/l culture). The mutant proteins showed identical UV–visible and NMR spectroscopic features both in the reduced and oxidized states when compared with the wild-type protein (results not shown).

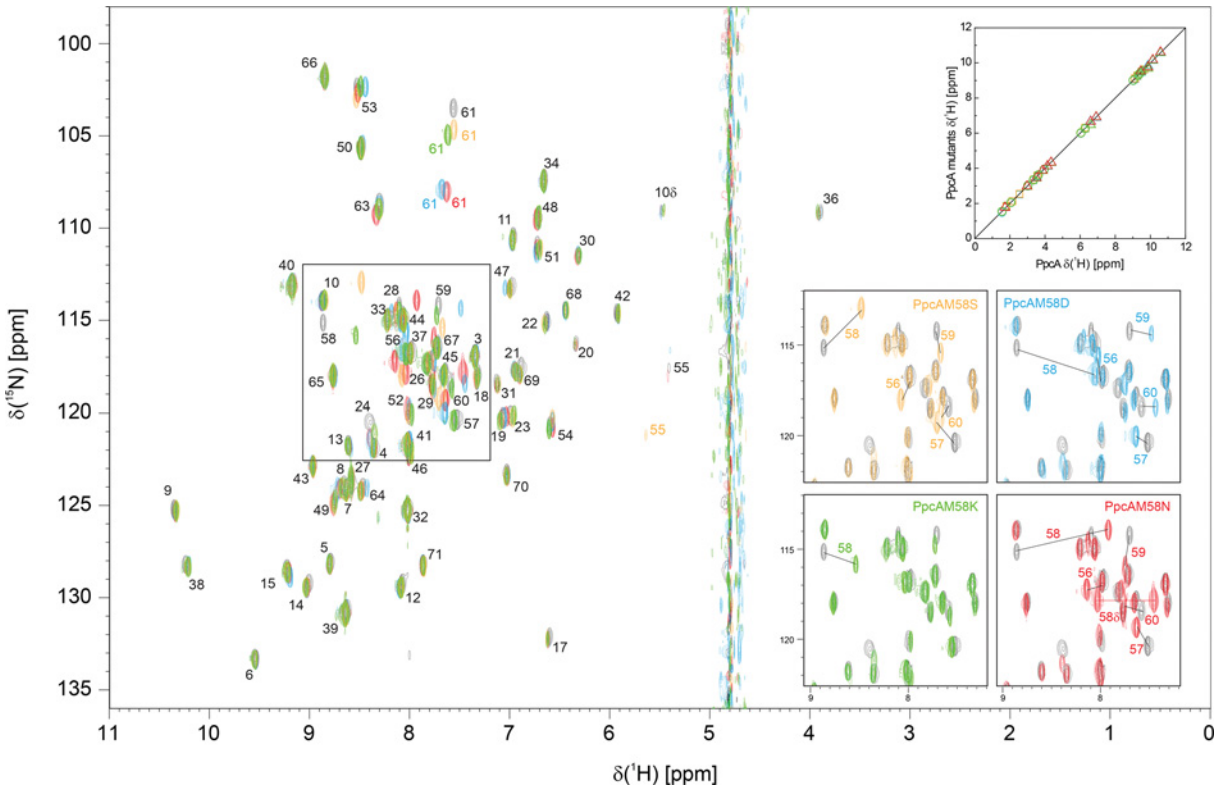

Figure 2 **2D-^{1}H-^{15}N HSQC NMR spectra of PpcAM58S (orange contours), PpcAM58D (blue contours), PpcAM58K (green contours), PpcAM58N (red contours) and PpcA (black contours)**

The most affected backbone amide signals are marked in the spectrum or in the expansion. The inset shows the comparison of the observed haem proton chemical shifts of reduced PpcAM58 mutants and those of PpcA. The symbols correspond to haem I (□), haem III (Δ) and haem IV (○). The colour code of the NMR spectra was used for each mutant. The rmsd between the chemical shifts measured for PpcAM58 mutants and those of PpcA are for haems I, III and IV, respectively 0.02; 0.03; 0.01 p.p.m. for PpcAM58S, 0.02; 0.03; 0.03 p.p.m. for PpcAM58D, 0.02; 0.07; 0.01 p.p.m. for PpcAM58K and 0.01; 0.05; 0.01 p.p.m. for PpcAM58N. The continuous line has a unit slope.

Chemical shifts are exquisitely sensitive probes of molecular structure and in the present work ^{1}H–^{15}N HSQC NMR experiments were used to fingerprint the overall structure of PpcAM58 mutants and to evaluate the impact of each mutation on the protein conformation. All backbone amides, except for the first two residues, were assigned for the wild-type protein [27] and the same methodology was used to assist in the assignment of PpcAM58 mutant signals. The comparison of the ^{1}H–^{15}N HSQC NMR spectra obtained for wild-type and each mutant show a similar dispersion of signals, indicating that the overall fold of the native protein is maintained (Figure 2). For all mutants the backbone amide signal of residue 58 is always the most affected one, showing the largest variation for mutant PpcAM58N. In general, the other affected amide signals, although to a smaller extent, correspond to residues located in the polypeptide segment His^{55}–Gly^{61}. Thus, it can be concluded that the replacement of Met^{58} residue led only to a small rearrangement of the neighbouring residues in this polypeptide segment without affecting the global fold of the protein. Depending on the mutation, the residues in this region are differently affected. For PpcAM58K, only backbone amide signals for residues Met^{58} and Gly^{61} are significantly affected. In case of PpcAM58D and PpcAM58S, the most affected residues are in the region Glu^{56}–Gly^{61} and His^{55}–Gly^{61}, respectively. On the other hand for PpcAM58N, the changes extended to residue Gly^{63} (covering the region His^{55}–Gly^{63}), indicating that replacement of methionine at position 58 by an asparagine residue involves more conformational rearrangements.

The impact of the mutations on the haem core architecture of the four PpcAM58 mutants was also probed by 2D ^{1}H-NMR; the haem proton resonances were assigned (Supplementary Table S1 at http://www.bioscirep.org/bsr/033/bsr033e002add.htm) and their chemical shifts were compared with those of the wild-type cytochrome (see inset in Figure 2) [13]. The rmsd (root mean square deviation) values between the chemical shifts for the wild-type and mutant cytochromes are low, although slightly higher for haem III signals in each case, as expected because of the close proximity of this haem to Met^{58}. The good correlation obtained in the chemical shifts of haem protons in the native and mutant proteins indicates that the neighbourhoods of each haem group were unaffected by the mutation. The NOE

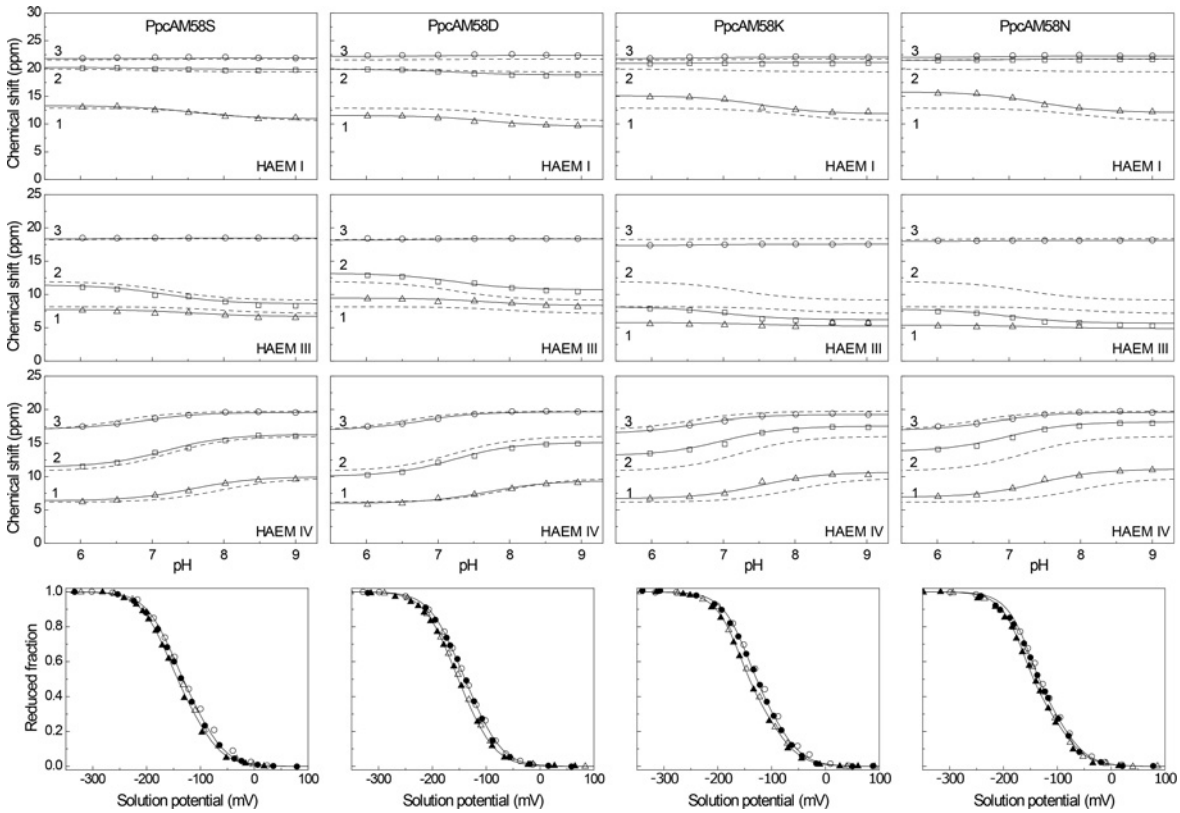

Figure 3 **Fitting of the thermodynamic model to the experimental data for PpcAM58 mutants**

The continuous lines are the result of the simultaneous fitting of the NMR and UV–visible data. The three upper panels show the pH dependence of haem methyl chemical shifts at oxidation stages 1 (△), 2 (□), and 3 (○). The broken lines in each panel represent the best fit for the wild-type protein. The chemical shift of the haem methyls in the fully reduced stage (stage 0) are not plotted since they are unaffected by the pH. The lower panel corresponds to the reduced fractions determined by UV–visible spectroscopy at pH 7 (○) and pH 8 (△). The open symbols and the filled symbols represent the data points in the reductive and oxidative titrations, respectively.

(nuclear Overhauser effect) connectivities between the haem groups were also analysed and showed the same set of connectivities for both the native and mutant proteins. Overall, these results demonstrated that the haem core arrangement is similar for all the proteins.

Redox characterization of haem groups and redox–Bohr centre

In order to probe the functional role of residue Met^{58} in the control of the redox properties and, concomitantly, in the global network of co-operativities, the detailed thermodynamic characterization of the four PpcAM58 mutants was carried out. The thermodynamic parameters of the wild-type protein were previously determined by fitting the pH-dependence of the chemical shifts of haem methyls $12^1CH_3{}^I$, $7^1CH_3{}^{III}$ and $12^1CH_3{}^{IV}$, measured in different stages of oxidation together with data from visible redox titrations obtained at pH 7 and 8, within the framework of an electrostatic model that considers four interacting centres: three haems and one protonatable centre [20]. In the present work, the same set of haem methyl groups were used to characterize the redox properties of PpcAM58 mutants. The NMR redox titrations followed by 2D-EXSY NMR spectroscopy showed that, as in the native cytochrome, the mutated proteins exhibit fast intramolecular and slow intermolecular electron exchange. To illustrate the stepwise oxidation of PpcAM58 mutants, 2D-EXSY NMR spectra obtained at pH 8 are shown in Supplementary Figure S3 (at http://www.bioscirep.org/bsr/033/bsr033e002add.htm). The same type of NMR spectra were collected at different pH values and the chemical shifts of haem methyls $12^1CH_3{}^I$, $7^1CH_3{}^{III}$ and $12^1CH_3{}^{IV}$ were measured for different oxidation stages (Figure 3). As for the fully reduced form (Supplementary Table S1), in the fully oxidized state (oxidation stage 3) the chemical shifts of the haem methyls of PpcA and PpcAM58 mutants are little affected (cf. open circles in each mutant with the correspondent dashed line in Figure 3). However, in the intermediate oxidation stages (stages 1 and 2) different scenarios were observed within the family of mutants. With exception of PpcAM58S, the chemical shifts of the haem methyls are quite different, in particular for those of haem III (Figure 3). By having essentially unaffected chemical shifts in the fully reduced and fully oxidized forms, the variations on

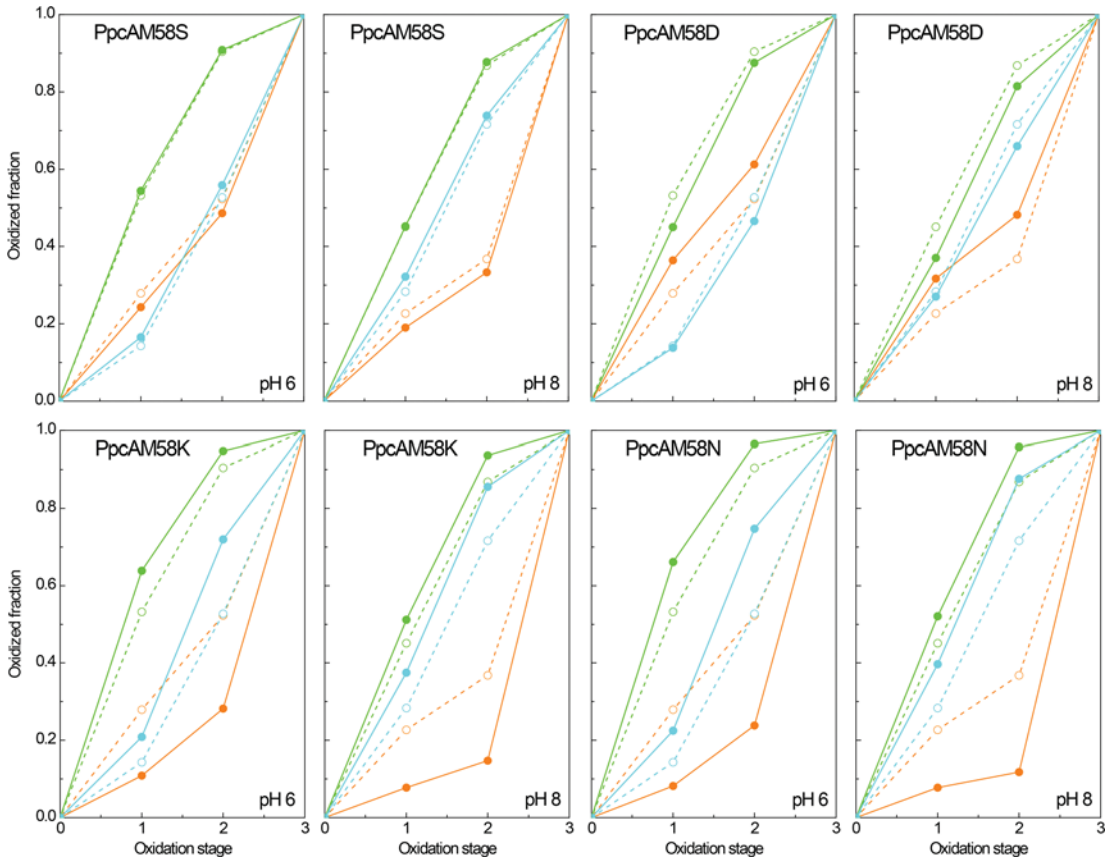

Figure 4 Oxidation fraction of PpcAM58 mutants (solid symbols and continuous lines) and PpcA (open symbols and broken lines) at pH 6 and pH 8

Haem I, III and IV data are coloured in green, orange and blue, respectively. The haem oxidation fractions were calculated according to equation $x_i = (\delta_i - \delta_0)/(\delta_3 - \delta_0)$, where δ_i, δ_0 and δ_3 are the observed chemical shifts of each methyl in stage i, 0 and 3, respectively.

the chemical shifts at intermediate oxidation stages reflect important changes in the haem oxidation fractions during the oxidation of the proteins, i.e., changes in their redox parameters. As an example, the oxidation pattern of the haem groups of the mutant and wild-type cytochromes at pH 6 and 8 are indicated in Figure 4. The comparison between the haem oxidation fractions in the mutant and in the wild-type cytochromes shows that, with exception of PpcAM58S, the haem oxidation profiles at both pH values were significantly altered with haem III being the most affected one (cf. broken and continuous lines in Figure 4). The haem III oxidation fractions are clearly higher in PpcAM58D when compared with the wild-type protein, whereas those of PpcAM58K and PpcAM58N are significantly smaller.

In order to quantify the effect of the mutations on the redox properties of the haem groups, the thermodynamic model was fitted to the pH-dependence of the observed chemical shift of haem methyls, together with data from visible redox titrations (see the Materials and methods section). The thermodynamic parameters are indicated in Table 1. The quality of the fittings obtained for the pH-dependence of the paramagnetic chemical shifts and for the visible redox titrations clearly shows that the experimental data is well described by the model (Figure 3). In the four mutants, the redox and redox–Bohr interactions are weaker compared with those of PpcA (Table 1). However, as observed for PpcA, the smallest redox interactions are established between the haems that are structurally further apart (haems I and IV), and the strongest redox–Bohr interactions with haem IV. The lower values of the redox interactions, in the context of a conserved haem core, might have their origin on structural rearrangements of charged groups that cause variations in local dielectric constants [32]. The positive values of the redox interactions indicates that the oxidation of a particular haem renders the oxidation of its neighbours more difficult, which is expected on an electrostatic basis due to the repulsion between the electron negative charges. Similarly, the negative redox–Bohr interactions (between the haems and the redox–Bohr centre) indicate that the oxidation of the haems facilitates the deprotonation of the redox–Bohr centre and vice versa. The higher redox–Bohr interaction observed with haem IV in Met^{58} mutants, indicates that the redox–Bohr centre remains associated with haem IV, as observed in the native protein [13,14,20].

Table 1 Thermodynamic parameters for PpcAM58 mutants
All energies are reported in meV, with standard errors given in parenthesis. For comparison the values previously obtained for PpcA [20] were also included. For each cytochrome, the fully reduced and protonated protein was taken as reference. Diagonal values (in bold) correspond to oxidation energies of the haems and deprotonating energy of the redox–Bohr centre. Off-diagonal values are the redox (haem–haem) and redox-Bohr (haem–proton) interactions energies.

	Energy (meV)			
Mutant	**Haem I**	**Haem III**	**Haem IV**	**Redox–Bohr centre**
PpcAM58S				
Haem I	**– 159 (4)**	17 (2)	6 (2)	– 13 (4)
Haem III		**– 139 (3)**	30 (2)	– 10 (4)
Haem IV			**– 131 (2)**	– 37 (4)
Redox–Bohr centre				**495 (8)**
PpcAM58D				
Haem I	**– 161 (4)**	18 (2)	6 (2)	– 18 (3)
Haem III		**– 156 (4)**	29 (2)	– 18 (3)
Haem IV			**– 134 (4)**	– 44 (3)
Redox–Bohr centre				**465 (7)**
PpcAM58K				
Haem I	**– 150 (4)**	8 (3)	– 2 (3)	– 18 (4)
Haem III		**– 109 (4)**	26 (3)	– 16 (4)
Haem IV			**– 123 (4)**	– 43 (4)
Redox–Bohr centre				**457 (7)**
PpcAM58N				
Haem I	**– 153 (3)**	– 4 (3)	– 9 (3)	– 11 (3)
Haem III		**– 103 (3)**	25 (3)	– 7 (3)
Haem IV			**– 126 (3)**	– 38 (3)
Redox–Bohr centre				**444 (5)**
PpcA				
Haem I	**– 154 (5)**	27 (2)	16 (3)	– 32 (4)
Haem III		**– 138 (5)**	41 (3)	– 31 (4)
Haem IV			**– 125 (5)**	– 58 (4)
Redox–Bohr centre				**495 (8)**

With the exception of PpcAM58S, the most affected haem reduction potential was that of haem III in the other mutants (Table 1). However, the reduction potential of haem III in these three mutants was differently affected. In PpcAM58D it decreased by 18 mV, whereas in PpcAM58K and PpcAM58N it is increased by 29 and 35 mV, respectively, in the fully reduced and protonated proteins. The variations observed suggest an important role for residue Met^{58} in the regulation of haem III properties.

Impact of the mutations on the haem oxidation order at physiological pH

The reduction potential of each haem group is affected by the oxidation state of neighbouring haems (redox interactions) and by the solution pH (redox–Bohr interactions). To evaluate the effect of the mutations on the haem midpoint reduction potentials (E_{app}, i.e. the point at which the oxidized and reduced fractions of each haem are equally populated) at physiological pH, the oxidation curves of the individual haems were computed from the thermodynamic parameters listed in Table 1. As for the wild-type protein, the redox interactions modulate the electron affinity of each haem so that the curves are non-Nernstian, showing some cross over during the redox titration (Figure 5). The mutant PpcAM58S shows similar haem oxidation profiles compared with the wild-type protein, which reflects their comparable redox parameters. Both proteins displayed the same haem oxidation order (I–IV–III) with the separation of the curves only slightly affected: the difference between the E_{app} values of haems I and IV decreased by 6 mV and that between haems IV and III increased by 11 mV in the mutant (Table 2). By contrast, the haem oxidation profiles of PpcAM58D show a general lowering of the E_{app} values of the haem groups compared with those of the wild-type protein. A significant decrease in the reduction potential is observed for haem III. This haem is more oxidized at low reduction potentials, i.e., in earlier stages of oxidation compared with PpcA (cf. Figures 4 and 5). Consequently, its E_{app} is nearly identical with that of haem IV and the haem oxidation order is I–(IV, III). On the other hand, in the mutant PpcAM58K, the positively charged lysine residue caused a significant alteration of E_{app} of haem III but in an opposite direction to that observed in PpcAM58D. Indeed, for PpcAM58K, the oxidation curve of haem III is well separated from those of the other haems at low reduction potentials

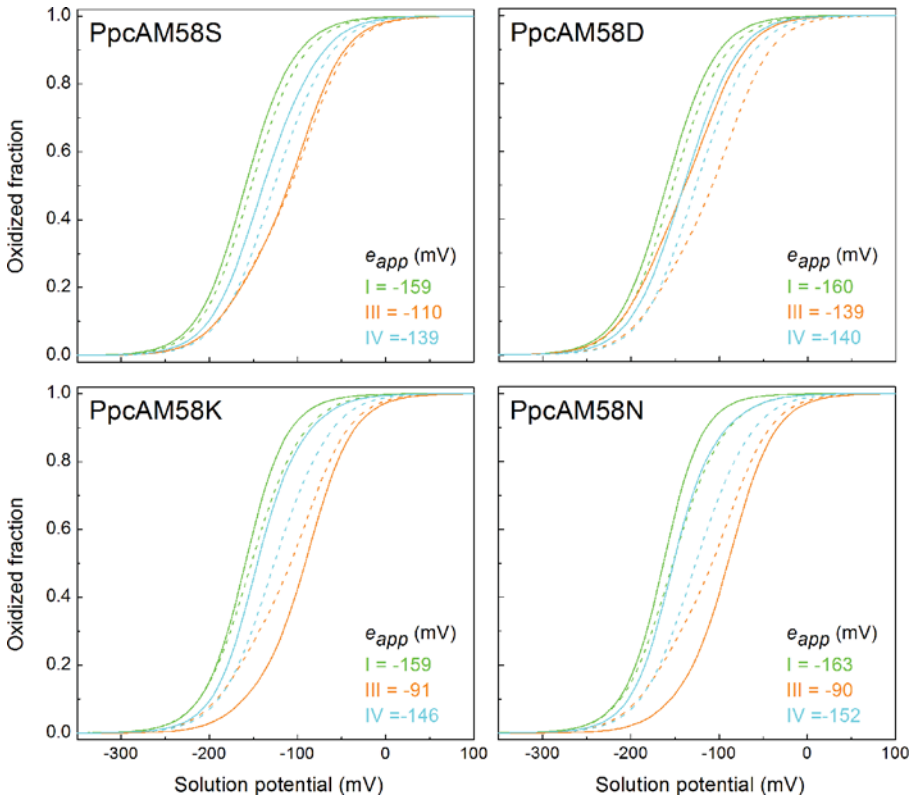

Figure 5 Oxidized fractions of the individual haems for PpcAM58 mutants (continuous lines) and wild-type (broken lines) at pH 7.5

The curves were calculated as a function of the solution reduction potential using the parameters listed in Table 1. The midpoint reduction potentials (E_{app}) of the haems are also indicated. The E_{app} values of PpcA were previously reported [20] and are −152 mV (haem I); −108 mV (haem III); and −126 mV (haem IV).

(Figure 5). Increasing the solution potential leads to the progressive oxidation of haems I and IV, which have negligible redox interaction, while keeping haem III essentially reduced. As a result, the oxidation curve of haem IV is basically unaffected by the oxidation of haem III, and hence, unaltered by the stronger interaction between these haems (Table 1), as it was in the wild-type protein. The actual order of the midpoint reduction potentials in PpcAM58K is I–IV–III, as observed for PpcA. However, despite showing the same order of oxidation, the difference between the E_{app} values of haems III and IV, in the case of PpcAM58K, is 37 mV higher compared with the wild-type (Table 2). The haem oxidation profiles of PpcAM58N (Figure 5) are similar to those of PpcAM58K as a result of the similarity of their thermodynamic parameters (Table 1). However, in PpcAM58N the difference between the E_{app} values of haems III and IV is 44 mV higher compared with the wild-type (Table 2). The results obtained for PpcAM58D and PpcAM58K can be rationalized on a pure electrostatic basis. Indeed, the replacement of a neutral methionine residue with negatively charged aspartic acid is expected to stabilize the oxidized form of the nearest haem (haem III) by lowering its reduction potential, whereas the opposite effect is expected by the introduction of a positive charge, as observed in PpcAM58K. On the other hand, it is rather striking that the neutral asparagine side chain at position 58 has a similar effect as the positively charged lysine residue, whereas the neutral serine residue has similar reduction potentials as the native. A structural model generated *in silico* (not shown) by mutating Met^{58} to Asn^{58} starting with solution structure of PpcA (PDB code 2LDO [14]) has revealed a possible hydrogen bond between main chain nitrogen atom of Lys^{60} and OD1 of Asn^{58}. The partial positive charge on the amide nitrogen of the side chain can interact with the π-electron cloud of haem III. The asparagine side chain will be within van der Waals contact of haem III. This observation is also corroborated by the chemical shift values of Asn^{58} γNH_2 side chain protons. The two protons are bonded to the same nitrogen atom and their identification is straightforward in the ^{1}H–^{15}N HSQC spectrum (see red straight line connecting these signals in PpcAM58N inset in Figure 2). The chemical shifts of Asn^{58} amide protons are 8.04 and 7.46 p.p.m., which are shifted to downfield from their average positions at 7.35 and 7.14 p.p.m. calculated from approximately 10^4 shifts as reported in the Biological Magnetic Resonance Data Bank (http://www.bmrb.wisc.edu/). Since in PpcA the non-haem aromatic rings, (Phe^{15} and Phe^{41}) are in distant regions in relation to Asn^{58} amide protons, the observed

Table 2 Comparison of the results obtained from the thermodynamic characterization of PpcAM58 mutants
For comparison the values previously obtained for PpcA and PpcD [20] were also included. ΔE_{app} (2nd/1st) is the difference between the E_{app} values of the second and the first haem to oxidized; ΔE_{app} (3rd/2nd) is the difference between the E_{app} values of the third and second haem to oxidized.

Protein	Order of haem oxidation	ΔE_{app} (2nd/1st) (mV)	ΔE_{app} (3rd/2nd) (mV)	Electron transfer pathway
PpcA	I-IV-III	26	18	$P_{0H}\rightarrow P_{1H}\rightarrow P_{14}\rightarrow P_{134}$
PpcAM58S	I-IV-III	20	29	$P_{0H}\rightarrow P_{1H}\rightarrow P_{14}\rightarrow P_{134}$
PpcAM58D	I-(III,IV)	20	1	No preferential pathway
PpcAM58K	I-IV-III	13	55	$P_{0H}\rightarrow P_{14}\rightarrow P_{134}$
PpcAM58N	I-IV-III	11	62	$P_{0H}\rightarrow P_{14}\rightarrow P_{134}$
PpcD	IV-I-III	6	54	$P_{0H}\rightarrow P_{14}\rightarrow P_{134}$

chemical shift of these protons can only be explained by the ring-current chemical shift contribution from haem III.

Role of Met^{58} on the functional mechanism of PpcA

As shown above, the oxidation profile of the redox centres is highly dependent on the nature of the side chain at position 58. In order to evaluate the effect of the mutation on the e^-/H^+ transfer mechanism of PpcA, the relative contribution of each of the 16 possible microstates (see Supplementary Figure S1) was determined as function of the solution potential for each mutant (Figure 6). Such study was previously done for the wild-type protein and a coherent electron transfer pathway coupled to proton transfer was established [20]. The relative variation of the microstates in PpcA is also depicted in Figure 6 together with those obtained in the present work for PpcAM58 mutants. While in the wild-type protein a concerted e^-/H^+ transfer occurs between oxidation stages 1 and 2, it is clear that the relative contributions of different microstates to the overall population in each stage are significantly altered in PpcAM58D, PpcAM58K and PpcAM58N (Figure 6). In fact, in the wild-type cytochrome the oxidation stage 0 is dominated by the fully reduced and protonated form P_{0H} and stage 1 is dominated by the oxidation of haem I (P_{1H}) while keeping the redox–Bohr centre protonated. Oxidation stage 2 is dominated by the oxidation of haems I and IV and deprotonation of the acid–base centre (P_{14}) that remains deprotonated in stage 3 upon full oxidation of haem III (P_{134}). Therefore a route is defined for electron transfer in PpcA: $P_{0H} \rightarrow P_{1H} \rightarrow P_{14} \rightarrow P_{134}$. Although the binding partners of PpcA are presently unknown, the functional, structural and backbone dynamics studies on PpcA suggest that haems I and IV might have a role in recognition of PpcA redox partners [14,20]. Since haem I is oxidized in the two functional microstates, it is most probable that the haem I region of PpcA interacts with its electron acceptor. Haem IV, which alters its oxidation state between the one- and two electron-oxidized proteins, is very likely the interaction region with the electron donor [14]. A hypothetical functional mechanism was recently proposed for the interaction between PpcA and its upstream partner [33].

Despite the higher contribution of microstate P_{14} in oxidation stage 2, compared with PpcA, this selected pathway is unaffected in PpcAM58S but is disrupted in PpcAM58D, PpcAM58K and PpcAM58N. In the PpcAM58D mutant, the mutation brings the midpoint reduction potential values of all haem groups closer to each other (cf. broken and continuous lines on Figure 5). Consequently, two microstates (P_{1H} and P_{3H}) are now dominant in the first oxidation stage and, thus, no preferential pathway for electron transfer is observed (Figure 6). On the other hand, in PpcAM58K and PpcAM58N a different mechanism for preferential electron transfer is established. In this case, the oxidation stage 0 is also dominated by the protonated form P_{0H}, but the microstates of oxidation stage 1 are overcome by the P_{14} curve, which intercepts earlier the curve of microstate P_{0H}. The microstate P_{14} dominates the oxidation stage 2, whereas P_{134} dominates stage 3. Thus, in these two mutants, a different preferential route for electrons is established, favouring a proton-coupled $2e^-$ transfer step between oxidation stages 0 and 2: $P_{0H} \rightarrow P_{14} \rightarrow P_{134}$.

Taken together, these observations and the relative E_{app} values of the haem groups, it is clear that haem III plays a key role in the functional mechanism of each cytocrome. Protein surroundings near haem III control its reduction potential relative to the other two haems, which in turn controls the microscopic redox states that can be accessed during the redox cycle, establishing preferential pathways for electron transfer. It is striking to note that one residue (Met^{58}) can fine tune the redox states that can be accessed by the protein enough to alter the functional pathways. Indeed, the replacement of the neutral side chain by the negatively charged one in PpcAM58D mutant altered the reduction potential of haem III in a way that this haem is no longer the last one to oxidize. In this case, the preferential pathway for e^-/H^+ transfer is altered. In mutant PpcAM58K, the introduction of a positively charged side chain at position 58 lead to a higher stabilization of the oxidized form of haem III, compared with the other two haems, and a different preferred electron transfer pathway was established. In wild-type, PpcAM58N and PpcAM58K, the order of oxidation of the haem groups is maintained, but in the mutants a different functional mechanism emerges in which a $2e^-$ step coupled with proton transfer is observed.

In summary, the reduction potential of haem III relative to the other two haems seems to be crucial in enabling these proteins to couple electron transfer with deprotonation of the redox–Bohr centre (Table 2). In fact, only preferential e^-/H^+ pathways are established if haem III shows higher reduction potential. However, the pathway varies with the separation between the E_{app} values of haem III and its predecessor (haem IV) in the order of

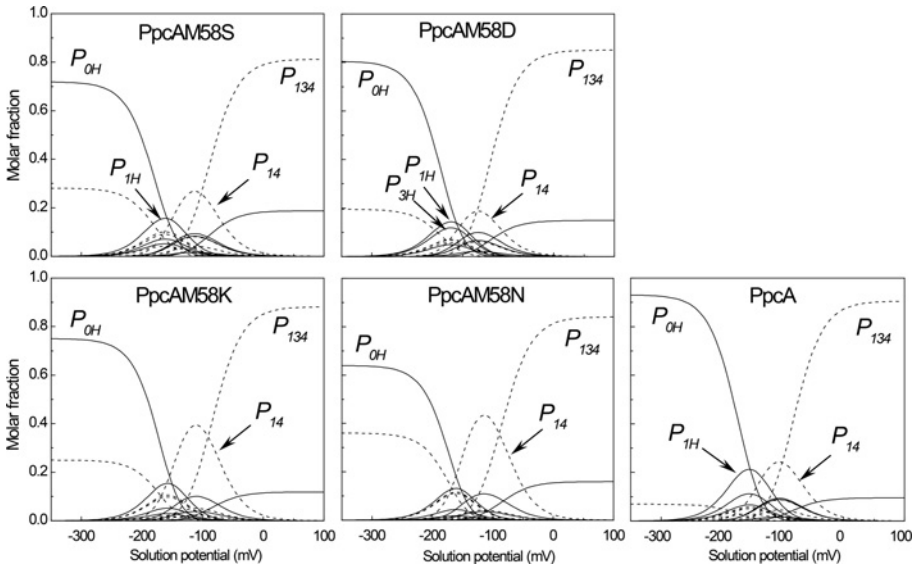

Figure 6 **Molar fractions of the 16 individual microstates of PpcAM58 mutants and wild-type cytochrome at pH 7.5**
The molar fractions were calculated as a function of the solution reduction potential using the parameters listed in Table 1. Continuous and broken lines indicate the protonated and deprotonated microstates (described in Supplementary Figure S1 at http://www.bioscirep.org/bsr/033/bsr033e002add.htm), respectively. For clarity only the relevant microstates are labelled.

oxidation (Table 2). In the case of PpcA such separation was 18 mV and the route for electron transfer was: $P_{0H} \rightarrow P_{1H} \rightarrow P_{14} \rightarrow P_{134}$. In the case of PpcAM58S the same route was observed but the slightly higher separation of the E_{app} values (29 mV against 18 mV in the wild-type) increased the contribution of microstate P_{14}. Finally, in PpcAM58K the higher separation between E_{app} values of haem III and haem IV (55 mV against 18 mV in the wild-type) lead to a significant contribution of the microstate P_{14} so that a different preferred route for electrons was observed: $P_{0H} \rightarrow P_{14} \rightarrow P_{134}$. This route was further reinforced in PpcAM58N, which shows a separation of 62 mV in E_{app} values of haems III and IV.

Interestingly, the results obtained from the thermodynamic characterization of the four *Gs* PpcA family homologues (PpcA, PpcB, PpcD and PpcE) have shown that only PpcA and PpcD, for which haem III has the highest reduction potential showed preferential pathways for electron/proton coupling [20]. Remarkably, in PpcD, for which oxidation order of the haem groups was I–IV–III and the difference between the E_{app} values of haems III and IV is comparable with that of PpcAM58K (54 mV in PpcD against 55 mV in the PpcAM58K), a similar electron transfer mechanism ($P_{0H} \rightarrow P_{14} \rightarrow P_{134}$) was observed.

Conclusions

In the present work, the role of residue Met^{58} on the redox properties of the trihaem cytochrome PpcA was studied by replacing it with serine, aspartic acid, asparagine or lysine. The results described show that Met^{58} is crucial in the regulation of the functional mechanism of PpcA, which is strongly dependent on the nature of the side chain at position 58. Indeed, the two mutants containing charged side chains, PpcAM58D and PpcAM58K affected significantly, albeit differently, the redox properties of the haems and altered the balance of the global network of cooperativities and the functional mechanism of the proteins. The data obtained suggests that the preferred e^-/H^+ transfer pathway observed for PpcA is strongly dependent on the reduction potential of haem III relative to the other haems and is favoured by a larger difference between the reduction potential of haem III and its predecessor. Overall, this study shows that the functional mechanism of PpcA relies on a fine-tuned balance of redox and redox–Bohr interactions that assure a coherent electron transfer pathway coupled to proton transfer, which allows the protein to perform e^-/H^+ energy transduction. The proper tuning of the reduction potentials is fundamental to achieve concerted e^-/H^+ transfer, which contributes to cellular energy transduction, which is intimately linked to the nature of the residue at position 58. The functional characterization of PpcA mutants as described in the present study opens up the possible development of strains carrying mutant cytochromes rationally designed to increase respiratory skills coupled to the cellular growth enhancement of *Gs*.

AUTHOR CONTRIBUTION

Carlos Salgueiro designed the study. Carlos Salgueiro and Leonor Morgado conducted and analysed the NMR experiments, calculated the thermodynamic parameters and wrote the paper. Leonor Morgado conducted the redox titrations followed by visible spectroscopy. Leonor Morgado, Joana Dantas and Telma Simões performed the bacterial growth and purification of PpcA M58 mutants.

Yuri Londer and P. Raj Pokkuluri provided the PpcA M58 mutant plasmids and key revisions of the paper.

ACKNOWLEDGMENT

We thank Professor D.L. Turner for providing us the software program used to calculate the thermodynamic parameters of the proteins.

FUNDING

This work was supported by the Fundação para a Ciência e Tecnologia (Portugal) [grant numbers PTDC/QUI/70182/2006, PEst-C/EQB/LA006/2011]. The NMR spectrometers are part of the National NMR Network (RNRMN) and are funded by the Fundação para a Ciência e a Tecnologia (FCT). The Met^{58} mutants were produced at ANL with support from U.S. Department of Energy Office of Biological and Environmental Research [grant numberDE-AC02-06CH11357]. The structural analysis of the mutants is supported by the division of Chemical Sciences, Geosciences, and Biosciences, Office of Basic Energy Sciences of the U.S. Department of Energy [grant number DE-AC02-06CH11357].

REFERENCES

1 Lovley, D. R., Ueki, T., Zhang, T., Malvankar, N. S., Shrestha, P. M., Flanagan, K. A., Aklujkar, M., Butler, J. E., Giloteaux, L., Rotaru, A. E. et al. (2011) *Geobacter*: the microbe electric's physiology, ecology, and practical applications. Adv. Microb. Physiol. **59**, 1–100

2 Lovley, D. R., Holmes, D. E. and Nevin, K. P. (2004) Dissimilatory Fe(III) and Mn(IV) reduction. Adv. Microb. Physiol. **49**, 219–286

3 Lovley, D. R. (2008) Extracellular electron transfer: wires, capacitors, iron lungs, and more. Geobiology **6**, 225–231

4 Anderson, R. T., Vrionis, H. A., Ortiz-Bernad, I., Resch, C. T., Long, P. E., Dayvault, R., Karp, K., Marutzky, S., Metzler, D. R., Peacock, A. et al. (2003) Stimulating the *in situ* activity of *Geobacter* species to remove uranium from the groundwater of a uranium-contaminated aquifer. Appl. Environ. Microbiol. **69**, 5884–5891

5 Gregory, K. B. and Lovley, D. R. (2005) Remediation and recovery of uranium from contaminated subsurface environments with electrodes. Environ. Sci. Technol. **39**, 8943–8947

6 Lloyd, J. R. and Lovley, D. R. (2001) Microbial detoxification of metals and radionuclides. Curr. Opin. Biotechnol. **12**, 248–253

7 Butler, J. E., Young, N. D. and Lovley, D. R. (2010) Evolution of electron transfer out of the cell: comparative genomics of six *Geobacter* genomes. BMC Genomics **11**, 40

8 Ding, Y. H., Hixson, K. K., Giometti, C. S., Stanley, A., Esteve-Núñez, A., Khare, T., Tollaksen, S. L., Zhu, W., Adkins, J. N., Lipton, M. S. et al. (2006) The proteome of dissimilatory metal-reducing microorganism *Geobacter sulfurreducens* under various growth conditions. Biochim. Biophys. Acta **1764**, 1198–1206

9 Methé, B. A., Nelson, K. E., Eisen, J. A., Paulsen, I. T., Nelson, W., Heidelberg, J. F., Wu, D., Wu, M., Ward, N., Beanan, M. J. et al. (2003) Genome of *Geobacter sulfurreducens*: metal reduction in subsurface environments. Science **302**, 1967–1969

10 Aklujkar, M., Krushkal, J., DiBartolo, G., Lapidus, A., Land, M. L. and Lovley, D. R. (2009) The genome sequence of *Geobacter metallireducens*: features of metabolism, physiology and regulation common and dissimilar to *Geobacter sulfurreducens*. BMC Microbiol. **9**, 109

11 Dantas, J. M., Morgado, L., Londer, Y. Y., Fernandes, A. P., Louro, R. O., Pokkuluri, P. R., Schiffer, M. and Salgueiro, C. A. (2012) Pivotal role of the strictly conserved aromatic residue F15 in the cytochrome c_7 family. J. Biol. Inorg. Chem. **17**, 11–24

12 Lloyd, J. R., Leang, C., Hodges Myerson, A. L., Coppi, M. V., Cuifo, S., Methe, B., Sandler, S. J. and Lovley, D. R. (2003) Biochemical and genetic characterization of PpcA, a periplasmic *c*-type cytochrome in *Geobacter sulfurreducens*. Biochem. J. **369**, 153–161

13 Morgado, L., Bruix, M., Orshonsky, V., Londer, Y. Y., Duke, N. E., Yang, X., Pokkuluri, P. R., Schiffer, M. and Salgueiro, C. A. (2008) Structural insights into the modulation of the redox properties of two *Geobacter sulfurreducens* homologous triheme cytochromes. Biochim. Biophys. Acta **1777**, 1157–1165

14 Morgado, L., Paixão, V. B., Schiffer, M., Pokkuluri, P. R., Bruix, M. and Salgueiro, C. A. (2012) Revealing the structural origin of the redox-Bohr effect: the first solution structure of a cytochrome from *Geobacter sulfurreducens*. Biochem. J. **441**, 179–187

15 Pessanha, M., Londer, Y. Y., Long, W. C., Erickson, J., Pokkuluri, P. R., Schiffer, M. and Salgueiro, C. A. (2004) Redox characterization of *Geobacter sulfurreducens* cytochrome c_7: physiological relevance of the conserved residue F15 probed by site-specific mutagenesis. Biochemistry **43**, 9909–9917

16 Pessanha, M., Morgado, L., Louro, R. O., Londer, Y. Y., Pokkuluri, P. R., Schiffer, M. and Salgueiro, C. A. (2006) Thermodynamic characterization of triheme cytochrome PpcA from *Geobacter sulfurreducens*: evidence for a role played in e^-/H^+ energy transduction. Biochemistry **45**, 13910–13917

17 Pokkuluri, P. R., Londer, Y. Y., Duke, N. E., Long, W. C. and Schiffer, M. (2004) Family of cytochrome c_7-type proteins from *Geobacter sulfurreducens*: structure of one cytochrome c_7 at 1.45 Å resolution. Biochemistry **43**, 849–859

18 Ding, Y. H., Hixson, K. K., Aklujkar, M. A., Lipton, M. S., Smith, R. D., Lovley, D. R. and Mester, T. (2008) Proteome of *Geobacter sulfurreducens* grown with Fe(III) oxide or Fe(III) citrate as the electron acceptor. Biochim. Biophys. Acta **1784**, 1935–1941

19 Shelobolina, E. S., Coppi, M. V., Korenevsky, A. A., Didonato, L. N., Sullivan, S. A., Konishi, H., Xu, H., Leang, C., Butler, J. E., Kim, B. C. et al. (2007) Importance of *c*-type cytochromes for U(VI) reduction by *Geobacter sulfurreducens*. BMC Microbiol. **7**, 16

20 Morgado, L., Bruix, M., Pessanha, M., Londer, Y. Y. and Salgueiro, C. A. (2010) Thermodynamic characterization of a triheme cytochrome family from *Geobacter sulfurreducens* reveals mechanistic and functional diversity. Biophys. J. **99**, 293–301

21 Pokkuluri, P. R., Londer, Y. Y., Yang, X., Duke, N. E., Erickson, J., Orshonsky, V., Johnson, G. and Schiffer, M. (2010) Structural characterization of a family of cytochromes c_7 involved in Fe(III) respiration by *Geobacter sulfurreducens*. Biochim. Biophys. Acta **1797**, 222–232

22 Morgado, L., Bruix, M., Londer, Y. Y., Pokkuluri, P. R., Schiffer, M. and Salgueiro, C. A. (2007) Redox-linked conformational changes of a multiheme cytochrome from *Geobacter sulfurreducens*. Biochem. Biophys. Res. Commun. **360**, 194–198

23 Londer, Y. Y., Pokkuluri, P. R., Tiede, D. M. and Schiffer, M. (2002) Production and preliminary characterization of a recombinant triheme cytochrome c_7 from *Geobacter sulfurreducens* in *Escherichia coli*. Biochim. Biophys. Acta **1554**, 202–211

24 Arslan, E., Schulz, H., Zufferey, R., Kunzler, P. and Thöny-Meyer, L. (1998) Overproduction of the *Bradyrhizobium japonicum c*-type cytochrome subunits of the cbb_3 oxidase in *Escherichia coli*. Biochem. Biophys. Res. Commun. **251**, 744–747

25 Fernandes, A. P., Couto, I., Morgado, L., Londer, Y. Y. and Salgueiro, C. A. (2008) Isotopic labeling of *c*-type multiheme cytochromes overexpressed in *E. coli*. Protein Expression Purif. **59**, 182–188
26 Wishart, D. S., Bigam, C. G., Yao, J., Abildgaard, F., Dyson, H. J., Oldfield, E., Markley, J. L. and Sykes, B. D. (1995) ^{1}H, ^{13}C and ^{15}N chemical shift referencing in biomolecular NMR. J. Biomol. NMR **6**, 135–140
27 Morgado, L., Paixão, V. B., Salgueiro, C. A. and Bruix, M. (2011) Backbone, side chain and heme resonance assignments of the triheme cytochrome PpcA from *Geobacter sulfurreducens*. Biomol. NMR Assign. **5**, 113–116
28 Goddard, T. D. and Kneller, D. G. (2007) Sparky 3.114, University of California, San Francisco, U.S.A
29 Turner, D. L., Salgueiro, C. A., Catarino, T., LeGall, J. and Xavier, A. V. (1996) NMR studies of cooperativity in the tetrahaem cytochrome c_3 from *Desulfovibrio vulgaris*. Eur. J. Biochem. **241**, 723–731
30 Salgueiro, C. A., Turner, D. L., Santos, H., LeGall, J. and Xavier, A. V. (1992) Assignment of the redox potentials to the four haems in *Desulfovibrio vulgaris* cytochrome c_3 by 2D-NMR. FEBS Lett. **314**, 155–158
31 Santos, H., Moura, J. J., Moura, I., LeGall, J. and Xavier, A. V. (1984) NMR studies of electron transfer mechanisms in a protein with interacting redox centres: *Desulfovibrio gigas* cytochrome c_3. Eur. J. Biochem. **141**, 283–296
32 Louro, R. O., Catarino, T., Paquete, C. M. and Turner, D. L. (2004) Distance dependence of interactions between charged centres in proteins with common structural features. FEBS Lett. **576**, 77–80
33 Morgado, L., Dantas, J. M., Bruix, M., Londer, Y. Y. and Salgueiro, C. A. (2012) Fine tuning of redox networks on multiheme cytochromes from *Geobacter sulfurreducens* drives physiological electron/proton energy transduction. Bioinorg. Chem. Appl. **2012**, 9

Received 31 July 2012/17 August 2012; accepted 20 August 2012

Published as Immediate Publication 2 October 2012, doi 10.1042/BSR20120086

Biosci. Rep. (2013) / **33** / art:e00002 / doi 10.1042/BSR20120086

OPEN ACCESS

Original Paper

SUPPLEMENTARY DATA

Role of Met^{58} in the regulation of electron/proton transfer in trihaem cytochrome PpcA from *Geobacter sulfurreducens*

Leonor MORGADO*, Joana M. DANTAS*, Telma SIMÕES*, Yuri Y. LONDER†[1], P. Raj POKKULURI† and Carlos A. SALGUEIRO*[2]

*Requimte-CQFB, Departamento de Química, Faculdade de Ciências e Tecnologia, Universidade Nova de Lisboa, Campus Caparica, 2829–516 Caparica, Portugal, and †Biosciences Division, Argonne National Laboratory, Argonne, IL 60439, U.S.A.

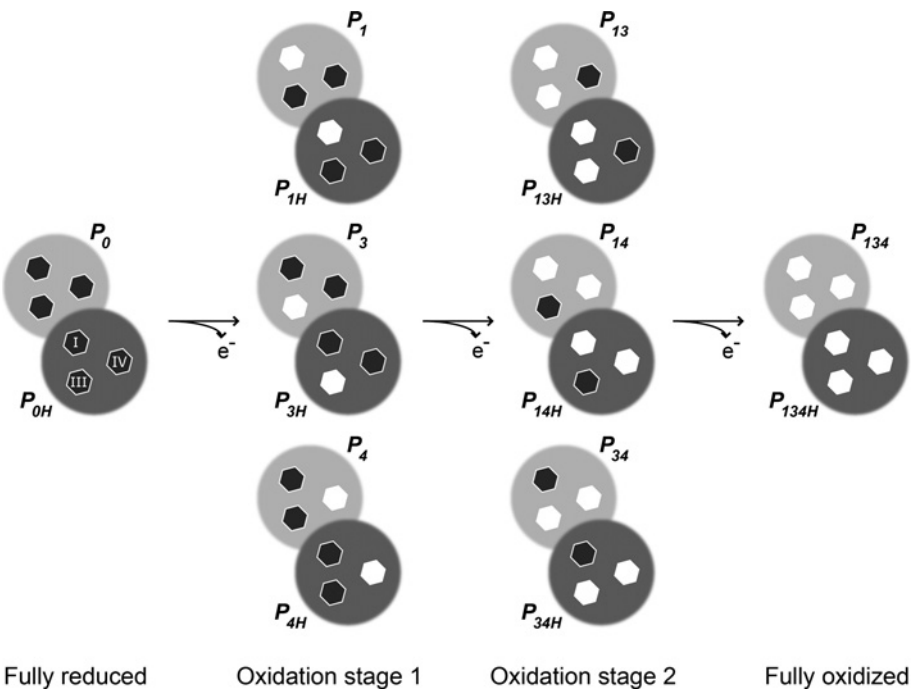

Figure S1 **Electronic distribution scheme for a trihaem cytochrome with a proton-linked equilibrium showing the 16 possible microstates**

The dark grey and light grey circles correspond to the protonated and deprotonated microstates, respectively. Hexagons represent haem groups, which can be either reduced (black) or oxidized (white). The microstates are grouped, according to the number of oxidized haems, in four oxidation stages connected by three one-electron redox steps. P_{0H} and P_0 represent the reduced protonated and deprotonated microstates, respectively. P_{ijkH} and P_{ijk}, indicate, respectively, the protonated and deprotonated microstates, where *i*, *j* and *k* represent the haem(s) that are oxidized in that particular microstate.

[1] Present address: New England Biolabs, 240 County Road, Ipswich, MA 01938, U.S.A.

[2] To whom correspondence should be addressed (email csalgueiro@fct.unl.pt).

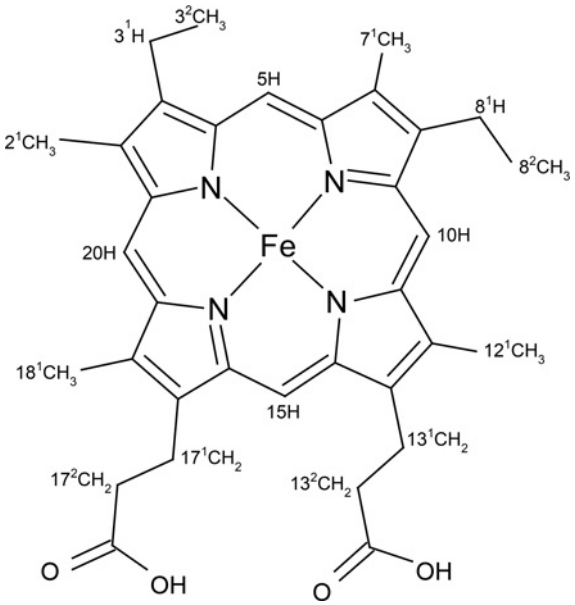

Figure S2 Diagram of a haem c numbered according to the IUPAC–IUB nomenclature [1]

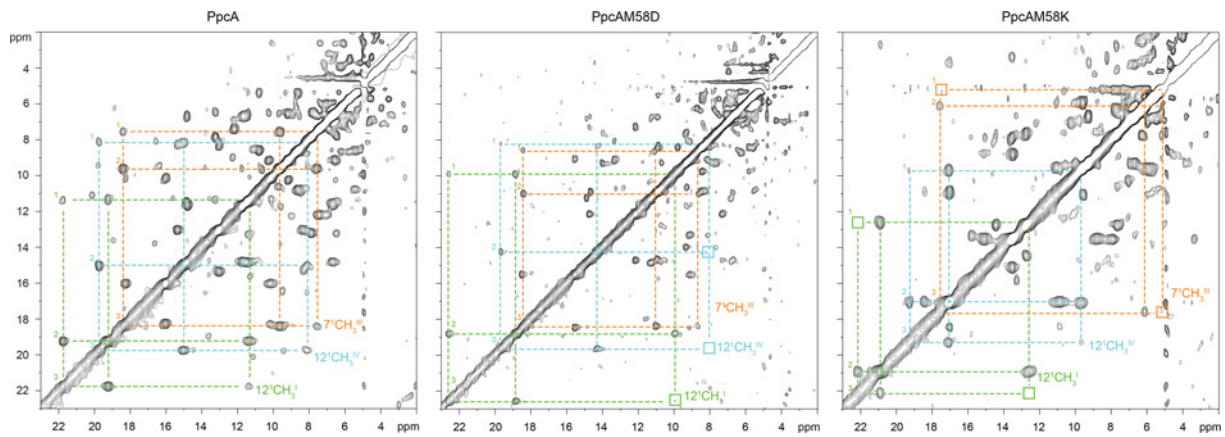

Figure S3 Expansions of 2D-EXSY NMR spectra obtained for PpcA and PpcAM58D and PpcAM58K at different levels of oxidation (288 K and pH 8)

2D-EXSY NMR spectra of PpcAM58S and PpcAM58N are similar to those of PpcA and PpcAM58K and are not represented. Cross-peaks resulting from intermolecular electron transfer between the the oxidation stages 1–3 are indicated for the haem methyls $12^1CH_3{}^{I}$ (green broken lines), $7^1CH_3{}^{III}$ (orange broken lines) and $12^1CH_3{}^{IV}$ (blue broken lines). Roman and Arabic numbers indicate the haems and the oxidation stages, respectively. In order not to overcrowd the Figure, the 2D-EXSY NMR spectra with cross-peaks to oxidation stage 0 are not shown. The chemical shifts corresponding to the oxidation stage 0 for each haem methyl are listed in Supplementary Table 1.

Table S1 Chemical shifts (p.p.m.) of the haem protons of PpcAM58 mutants in the reduced state at pH 8.0 and 288 K
For comparison chemical shift values obtained for PpcA [2] are indicated in parentheses.

Haem substituent	Mutant	Haem I	Haem III	Haem IV
5H	M58D	9.61 (9.65)	10.57 (10.58)	9.00 (9.02)
	M58K	9.64	10.58	9.01
	M58S	9.63	10.58	9.01
	M58N	9.63	10.61	9.01
10H	M58D	9.08 (9.12)	9.84 (9.86)	9.31 (9.33)
	M58K	9.12	9.68	9.32
	M58S	9.12	9.82	9.31
	M58N	9.11	9.76	9.33
15H	M58D	9.25 (9.26)	9.47 (9.45)	9.50 (9.51)
	M58K	9.27	9.49	9.54
	M58S	9.28	9.49	9.54
	M58N	9.27	9.52	9.54
20H	M58D	9.49 (9.50)	10.14 (10.14)	9.38 (9.39)
	M58K	9.51	10.15	9.40
	M58S	9.51	10.14	9.39
	M58N	9.51	10.17	9.40
2^1CH_3	M58D	3.54 (3.56)	4.33 (4.35)	3.60 (3.61)
	M58K	3.56	4.32	3.62
	M58S	3.56	4.33	3.62
	M58N	3.56	4.33	3.62
7^1CH_3	M58D	3.56 (3.58)	4.11 (4.14)	3.00 (3.02)
	M58K	3.58	4.13	3.01
	M58S	3.58	4.13	3.02
	M58N	3.58	4.13	3.03
12^1CH_3	M58D	2.51 (2.55)	3.48 (3.50)	3.93 (3.95)
	M58K	2.55	3.44	3.94
	M58S	2.55	3.48	3.94
	M58N	2.54	3.45	3.95
18^1CH_3	M58D	3.33 (3.34)	3.87 (3.86)	3.33 (3.34)
	M58K	3.34	3.86	3.34
	M58S	3.35	3.86	3.35
	M58N	3.35	3.87	3.35
3^1H	M58D	6.28 (6.30)	6.89 (6.91)	6.00 (6.04)
	M58K	6.28	6.91	6.02
	M58S	6.28	6.91	6.03
	M58N	6.29	6.91	6.02
8^1H	M58D	6.26 (6.29)	6.68 (6.60)	6.26 (6.28)
	M58K	6.31	6.47	6.27
	M58S	6.31	6.66	6.26
	M58N	6.28	6.66	6.28
3^2CH_3	M58D	2.13 (2.14)	1.77 (1.73)	2.06 (2.06)
	M58K	2.13	1.77	2.05
	M58S	2.13	1.78	2.06
	M58N	2.13	1.77	2.06
8^2CH_3	M58D	1.79 (1.79)	2.97 (2.98)	1.49 (1.55)
	M58K	1.85	2.97	1.55
	M58S	1.83	2.95	1.54
	M58N	1.79	2.98	1.54

REFERENCES

1 Moss, G. P. (1988) Nomenclature of tetrapyrroles. Recommendations 1986 IUPAC–IUB Joint Commission on Biochemical Nomenclature (JCBN). Eur. J. Biochem. **178**, 277–328
2 Morgado, L., Bruix, M., Orshonsky, V., Londer, Y. Y., Duke, N. E., Yang, X., Pokkuluri, P. R., Schiffer, M. and Salgueiro, C. A. (2008) Structural insights into the modulation of the redox properties of two *Geobacter sulfurreducens* homologous triheme cytochromes. Biochim. Biophys. Acta **1777**, 1157–1165

Received 31 July 2012/17 August 2012; accepted 20 August 2012

Published as Immediate Publication 2 October 2012, doi 10.1042/BSR20120086